ISME

Iranian Journal of Mechanical Engineering
The Iranian Society of Mechanical Engineers
Research Paper

DOI: 10.30506/JMEE.2022.538146.1271

Rapid Subsonic Flutter Analysis for Low Aspect Ratio Composite Wings

M. Basiri[*]
Ph.D.

H. Farrokhfal[†]
Assistant Professor

M. Mosayebi[‡]
Associate Professor

R. Koohi[§]
Assistant Professor

This study aims to achieve effective analysis and fast modeling in free vibration and flutter analyses of low aspect ratio composite wings in subsonic flow for the preliminary design stage instead of using the computationally expensive finite element method. It uses an equivalent plate method for structural modeling. Also, it uses the doublet point and the U-g methods for calculation of unsteady aerodynamic loads and carrying out flutter analysis, respectively. We investigate the effects of different parameters on the flutter behavior. The present results confirm that the structural tailoring can make a harmonious balance to the wing sweep angle effect upon the flutter behavior of composite wings, and a considerable improvement upon flutter performance is achieved by using composite materials.

Keywords: Flutter, Equivalent plate, Composite, Doublet point method

1 Introduction

The field of aeroelasticity involves the mutual interaction among the aerodynamic, inertial, and elastic forces. Wing flutter phenomenon is a dynamic instability associated with the interaction of inertial, elastic, and aerodynamic forces, which generally leads to catastrophic structural failure [1].

Instead of the computationally expensive finite element analysis, the equivalent plate method has been used in initial design phases or conceptual design of low-aspect-ratio aircraft wing structures. In the Ritz method-based equivalent plate method, the model characteristics are represented with polynomials as trial functions, which require only a few numbers of the input data, unlike a finite element model. In 1986 a Ritz method-based equivalent plate method was proposed at NASA Langley Research Center. In this method, the wing structure is modeled with several trapezoidal segments [2].

Aerodynamic calculations have a vital contribution to flutter analysis because structural deformations affect aerodynamic loads. The effects of elastic deformations at low flight speed

[*]Department of Mechanical Engineering, Malek-Ashtar University of Technology, Shahinshahr, Iran, M.Basiri@mut-es.ac.ir

[†]Corresponding Author, Department of Mechanical Engineering, Malek-Ashtar University of Technology, Shahinshahr, Iran, farrokhfal@mut-es.ac.ir

[‡]Department of Mechanical Engineering, Malek-Ashtar University of Technology, Shahinshahr, Iran, m.mosayebi@mut-es.ac.ir

[§]Department of Mechanical Engineering, Khomeinishahr Branch, Islamic Azad University, Khomeinishahr, Iran, koohi@iaukhsh.ac.ir

Receive: 2021/09/03 Accepted: 2022/02/17

are small. At high flight speed, elastic deformation may cause instability in a wing, or rendering a control surface ineffective, or even control reversal [3].

Several researchers have presented unsteady aerodynamic theories for deriving the pressure distribution on a thin finite wing in subsonic flow. Kussner [4] proposed an integral equation. The mode function methods and the direct element methods are two principal categories that include all available methods. Watkins et al. [5] improved the mode function method practically. Redman and Rowe [6] obtained the unsteady pressure distribution on wings with control surfaces successfully. The doublet lattice method is a common discrete-element method type [7-9]. This well-known method can be used readily to complex wing configurations. The existence of an inconsistency in the steady-state part is the disadvantage of this method [7]. Ueda and Dowell [10] formulated a doublet point method for calculating unsteady aerodynamic loads in subsonic flow on harmonically oscillating thin wings. This method is based on the concept of concentrated loads. In other words, on aerodynamic elements, the lift distribution is replaced by concentrated lift forces.

Aeroelastic phenomena were solved with different theories. Hollowell and Dugundji [11] have investigated an analytical solution for aeroelastic analysis of unswept rectangular wings. The wings were simulated as plates with torsion-bending stiffness coupling. The obtained results by the analytical solution were verified by the experiment. Rayleigh-Ritz method was used for calculation of mass and stiffness matrices, and unsteady two-dimensional aerodynamic theory was used for calculation of aerodynamic loads in incompressible flow. The U-g method was used for divergence and flutter analyses, and the obtained results were compared to the results of low-speed wind tunnel tests. They concluded that negative stiffness coupling makes divergence in a wing, while positive coupling delays the happening of stall flutter.

Lin et al. [12] used the finite element method (FEM) with 18-degree-of-freedom triangular plate elements. They studied the effects of sweep angle, aspect ratio, orthotropic modulus ratio, and composite fiber angle on the free vibration, divergence, and flutter characteristics of cantilever plates fluttering in subsonic flow. The classical lamination theory of plates was used to obtain the mass and stiffness matrices of the wing structure. By using the doublet-lattice method and the lifting surface theory, unsteady aerodynamic loads were numerically calculated. A surface spline is utilized to interpolate to interconnect the aerodynamic control points and structural nodes. They concluded that noticeable improvement in flutter/ divergence performance could be reached by varying the orthotropic modulus ratio and proper selecting of fiber orientation. Also, they found that structural tailoring can make a harmonious balance to the wing sweep angle effect upon the aeroelastic stability behavior of a wing.

Koo and Lee [13] studied the effect of structural damping on the flutter boundary of rectangular and swept composite wings using the finite element method. By using the doublet point method, the aerodynamic loads on wings were calculated. A surface spline is utilized to Interpolate to interconnect the aerodynamic control points and structural nodes. The effects of composite filament angles on the divergence/flutter performances were studied. They concluded that the structural damping decreases the flutter frequency but it increases the flutter speed of a composite wing.

Abdelrahmen [14] investigated static and dynamic aeroelastic behavior of composite swept wings. He used a modified equivalent plate analysis based on classical and first-order plate theories. To exhibit the effect of wing aspect ratio, sweep angle, taper ratio, number of layers, and composite filament angles on the divergence, flutter, and control reversal phenomenon, a parametric study was performed. He concluded that by moving the principal skin stiffness direction ahead of the wing reference axis, it is possible to enhance divergence speed. Similarly, by moving the principal skin stiffness direction behind the wing reference axis, it is possible to improve flutter performances of back-swept wings. Dunn and Dugundji [15] investigated the nonlinear stalled aeroelastic performance of rectangular composite cantilever wings with

different amounts of torsion-bending stiffness coupling. Validation of the analytical model was performed by a wind-tunnel test.

Livne and Li [16] achieved analytical sensitivities of aeroservoelastic response according to parameters of wing and control surface planform shape. They used the doublet point lifting surface method and equivalent plate method for aerodynamic and structural analysis, respectively. He expanded an effective approximation approach to optimize wing shape as a multidisciplinary optimization method.

Lu and Huang [17] used active acoustic excitations to propose a theoretical method of the flutter suppression for thin oscillating airfoils in incompressible flow. A simple harmonic acoustic excitation was utilized to induce unsteady aerodynamic loads. These closed-form loads were calculated on a typical section model. The flutter analysis was investigated using both the root locus and U-g methods.

Na and Shin [18] proposed an equivalent plate method to calculate natural frequencies and mode shapes of a low-aspect-ratio semi-monocoque main composite wing, consisting of spars, ribs skins, and a control surface. It was a first-order shear deformation theory based method, and a FEM was employed as a solver.

Abbas et al. [19] utilized a Modified higher-order shear deformation theory and the Rayleigh-Ritz method for deriving the mass and stiffness matrices. Unsteady aerodynamic loads over the trapezoidal composite wings in subsonic flow were calculated by a Doublet point method. By using the U-g method, the flutter and divergence analyses were performed. The effect of composite filament angles on natural frequency, divergence and flutter speeds were investigated. They concluded that divergence does not happen in wings with positive composite filament angles, but the flutter speeds are lower than those of wings with negative composite filament angles. So, obtaining composite tailoring with high-flutter and high-divergence boundaries at the same time is not easy.

Jian et al. [20] presented a method of equivalent simplification, using equivalent-plate models. It was based on the assumption that the different plate units (such as rib web, beam web, skin) are not distinguished in modeling, which led to avoid the complex pre-processing and made it more generalized. Their method was based on the first-order shear deformation theory of plates. As trial functions, Legendre polynomials were applied in The Ritz method. Calculations of aerodynamic load and flutter analysis were performed using ZAERO software. The results of vibration and flutter analysis obtained using the equivalent-plate model agreed well with those obtained by the Finite Element Method.

Shokrollahi et al. [21] used the first-order shear deformation plate theory and a supersonic Mach box method to study flutter speeds of a low aspect ratio trapezoidal structurally hybrid wing from low supersonic velocities to moderate velocities. The main objective of this work was to study the effect of composite to metal spanwise length ratio of hybrid wing structure on flutter speeds. The effect of fiber orientation with various geometric parameters such as sweep angle, taper ratio was investigated on the flutter speed. They concluded that for specified geometric parameters, there exists an optimum metal to composite proportion at which the flutter speed is maximum. It was realized that for a specified taper ratio or sweep angle, there was a maximum flutter speed corresponding to an optimum fiber orientation in the composite part.

Babin et al. [22] presented a 2D plate model based on the fluid-structure interaction method and classical plate theory for the aeroelastic analysis of low aspect ratio composite wings. The supersonic loads and domain model were defined by first-order piston and Hamilton principle theories. By using the differential quadrature method literature, natural frequencies and flutter speeds were analyzed and verified. They concluded that the flutter characteristics are strongly dependent on cross-ply laminates. The effects of the aspect ratio on supersonic flutter performance of laminated wings were studied.

He and et al. [23] presented a wind tunnel testing for a three-dimensional wing model with a control surface. They introduced adjustable nonlinear freeplay into the control surface

deflection leaf spring. Also, they tested the experimental aeroelastic model in a wind tunnel up to the critical flutter speed or limit cycle oscillations.
Pohly and et al. [24] presented wing flutter analyses using computational fluid-structure interaction dynamics. The obtained results show the potential speed and accuracy of the computational method, which will allow designers to rapidly determine capable of safe operating of an aircraft within its design envelope.
In the present work, an equivalent plate method is used for structural modeling of low aspect ratio composite wings. The Rayleigh-Ritz method and first-order shear deformation theory are utilized for deriving the mass and stiffness matrices. Chebyshev polynomials are employed as the trial functions in the approximation of structural deformations. Boundary conditions are enforced by applying proper artificial springs. Unsteady aerodynamic loads over the composite wings in subsonic flow were calculated by a Doublet point method. Flutter analysis is performed using the U-g method. The effects of wing sweep angle, aspect ratio, composite filament angle, and orthotropic modulus ratio on the flutter behavior of composite wings in subsonic flow are studied. The presented approach can be applied to the vibration and flutter analyses of low aspect ratio composite wings. It is to achieve purposes of effective analysis and fast modeling in free vibration and flutter analysis of composite wings in the preliminary design stage instead of using the computationally expensive finite element method. The obtained results are validated with the results available in the literature. This equivalent plate model has not been so far used for an aeroelastic analysis by previously mentioned references. The combination of this equivalent plate model, doublet point, and U-g methods have been used to achieve a new algorithm for flutter analysis of low-aspect-ratio composite wings in the preliminary design stage instead of using the computationally expensive FEM. This new algorithm is very effective and rapid, and it requires only a few input data in comparison to a corresponding finite element model. Also, its runtime is smaller than the runtime of FEM. Therefore, effective analysis and fast modeling are the primary purposes of this paper.

2 Structural Modeling of a Wing by Using the Equivalent Plate Method

The boundary condition of the wing is assumed clamped at the root. The transverse deflection w_0 can be written as follows:

$$w_0(\xi,\eta,t) = \mathbf{a_3}(\xi,\eta)\mathbf{q_3}(t) \qquad (١)$$

where $\mathbf{q_3}(t)$ is the Rayleigh-Ritz coefficients vector of the displacement in the z direction, which is time-dependent. The vector of the trial functions in Ritz method, $\mathbf{a_3}$ is given by [25]:

$$\mathbf{a_3}(\xi,\eta) = \{T_0(\eta)T_0(\xi), T_0(\eta)T_1(\xi), T_0(\eta)T_2(\xi), ..., T_M(\eta)T_N(\xi)\} \qquad (٢)$$

in which T_i can be chosen to be the Chebychev polynomials. ξ and η are transformed coordinates.
The plate is transformed into a square region with vertices having values ranging from - 1 to 1, as shown in Figure (1).
The equation of motion is obtained from Hamilton's principle as follows [25]:

$$\mathbf{M\ddot{q} + Kq = F_{z0}} \qquad (3)$$

where **M** and **K** are the mass and stiffness matrices of the wing, respectively. $\mathbf{F_{z0}}$ is the column vector of the aerodynamic load on the wing, and **q** is the Rayleigh-Ritz coefficients vector of all displacements and rotations.

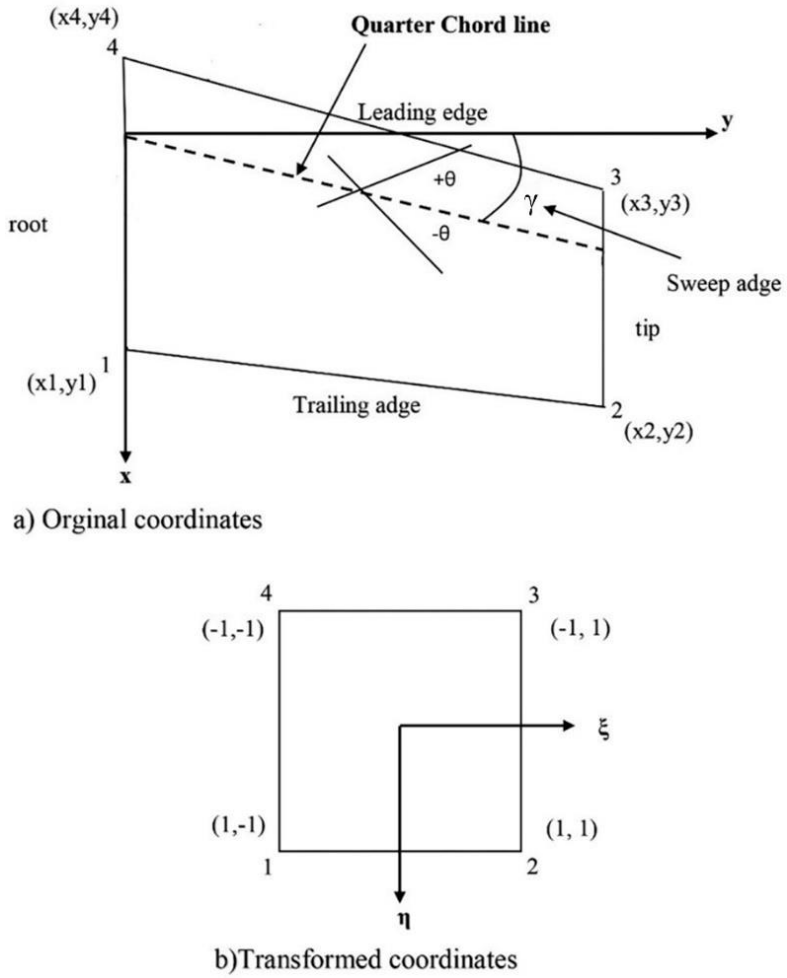

Figure 1 Plate definitions and transformed coordinates [25]

By adding all of the stiffness and mass matrices corresponding to each component, the stiffness matrix associated with the strain energy $\mathbf{K}_{strain}$ and the mass matrix of the entire wing $\mathbf{M}$ can be calculated [26]:

$$\mathbf{K}_{strain} = \mathbf{K}_{skin} + \mathbf{K}_{sapr} + \mathbf{K}_{rib} \quad (٤)$$

$$\mathbf{M} = \mathbf{M}_{skin} + \mathbf{M}_{spar} + \mathbf{M}_{rib} \quad (٥)$$

Chebychev polynomials don't satisfy the boundary conditions, and they are enforced by applying proper artificial springs [25]. The total stiffness matrix of the wing $\mathbf{K}$ is found to be the summation of the $\mathbf{K}_{strain}$ and the matrix associated with the boundary spring approximations $\mathbf{K}_{spring}$.

$$\mathbf{K} = \mathbf{K}_{strain} + \mathbf{K}_{spring} \quad (٦)$$

Other details and the equations used for structural modeling and calculating the stiffness and mass matrices of a semi-monocoque main wing, consisting of spars, skins, and ribs, are presented by Kapania and et al. [25, 26]. A series of convergence investigations on the number of terms k of the polynomials were performed by Lovejoy [27]. The conclusion is that, when more terms are used, the tendency of convergencies evident and when k =8 the first several modes are very close to convergence.

3 Unsteady Aerodynamic Formulation

The subsonic unsteady aerodynamic loads on two-dimensional wings are calculated by the doublet point method. In the doublet point method, the distributed aerodynamic loads are replaced by the concentrated loads vector $\mathbf{F_{z0}}$. The doublet point method can readily be coupled with aeroelastic analysis methods to perform flutter and divergence analysis. The relation between amplitudes of pressure distributions and their upwash velocity on oscillating lifting surfaces is written as follows [4, 10, 28]:

$$v_I(x,y) = \frac{1}{8\pi}\iint_s \Delta p(\xi,\eta) K(x_0,y_0)\,\mathrm{d}\xi\,\mathrm{d}\eta \qquad (٧)$$

As an assumption, the lifting surface is in the x-y plane (z = 0). The non-dimensional pressure coefficient Δ_p is written as follows:

$$\Delta p = \frac{-p'_+ + p'_-}{0.5\rho_\infty u_\infty^2} \qquad (8)$$

where p'_- and p'_+ are disturbance pressure of the lower and upper surfaces of a wing, respectively. Also, ρ_∞ and u_∞ are density and velocity of the uniform flow, respectively. The Kernel function $K(x_0,y_0)$ in Eq.(7) is defined as:

$$K(x_0,y_0) = e^{-ikx_0}\left[\frac{Me^{ikx}}{R\sqrt{x^2+r^2}} + B(k,r,x)\right] \qquad (٩)$$

The parameter r is absolute value of y_0. Other parameters of the Eq. (9) are presented by Ueda and Dowell [10]. The wing planform is partitioned into element surfaces so that the two side edges of each element are parallel to the uniform flow. Numbering the element surfaces and a focus on the i^{th} element have been shown in Figure (2).

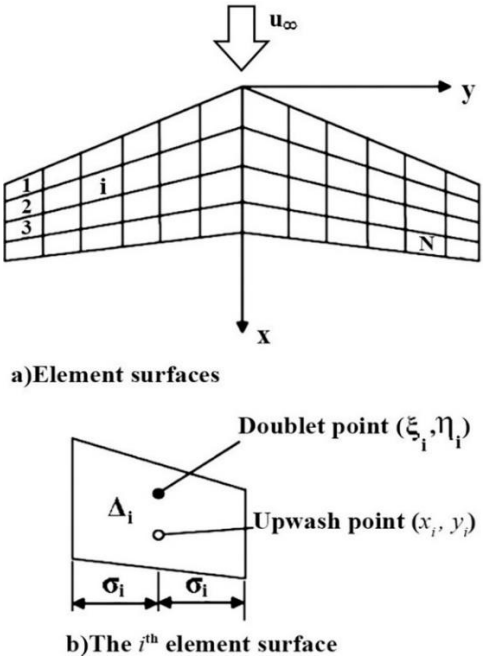

Figure 2 Element surfaces in the doublet point method [10]

The element surface has a width of $2\sigma_i$ and the area of Δ_i. In the doublet point method, the lift distribution on the i^{th} element surface is replaced by the equivalent concentrated load at the doublet point (ξ_i,η_i). The upwash distribution on the i^{th} element surface is replaced by the equivalent upwash at the upwash point (x_i,y_i). By considering these assumptions, the upwash of the i^{th} element surface in Eq. (7) is discretized and can be written as [10]:

$$v_I(x_i, y_i) = \frac{1}{8\pi}\sum_{j=1}^{N}\Delta p(\xi_j, \eta_j)\Delta_j K(x_i - \xi_j, y_i - \eta_j), (i = 1, 2, ..., N) \tag{10}$$

Equation (10) can be rewritten as:

$$\mathbf{v_I} = \mathbf{D}\mathbf{c_p} \tag{11}$$

where **D** is the matrix aerodynamic influence coefficients (AICs), $\mathbf{v_I}$ is the velocities induced at (x_i,y_i), and $\mathbf{c_p}$ is the vector of pressure coefficient, which is representative of the pressure coefficient at (ξ_i,η_i) and defined as follows:

$$\mathbf{v_I} = \{v_{Ii}\} = \{v_I(x_i, y_i)\} \tag{12}$$

$$\mathbf{D} = \left[d_{ij}\right] = \frac{\Delta_j}{8\pi}K(x_i - \xi_j, y_i - \eta_j) \tag{13}$$

$$\mathbf{c_p} = \{c_{pj}\} = \{\Delta p(\xi_j, \eta_j)\} \tag{14}$$

The upwash vector for the i^{th} element is calculated as [10]:

$$v_{Ii} = \frac{\partial}{\partial x}w_0(x_i, y_i) + ikw_0(x_i, y_i) \tag{15}$$

where $w_0(x_i,y_i)$ is the transverse deflection of the mid-plane at the upwash point of the i^{th} element surface.

$$v_{Ii} = (\mathbf{v_{IRi}} + i\mathbf{v_{IIi}})\mathbf{q_3} \tag{16a}$$

$$\mathbf{v_{IRi}} = \left\{\frac{\partial \mathbf{a_3}}{\partial x}(x_i, y_i)\right\} \tag{16b}$$

$$\mathbf{v_{IIi}} = k\{\mathbf{a_3}(x_i, y_i)\} \tag{16c}$$

The induced velocities for all elements are calculated as follows:

$$\mathbf{v_I} = \mathbf{v_{IT}}\mathbf{q_3} \tag{17a}$$

$$\mathbf{v_{IT}} = \mathbf{v_{IR}} + i\mathbf{v_{II}} \tag{17b}$$

By substituting $\mathbf{v_{IT}}$ from Eq. (17b) into Eq. (11), $\mathbf{c_p}$ is obtained as:

$$\mathbf{c_p} = \mathbf{D}^{-1}\mathbf{v_{IT}}\mathbf{q_3} \tag{18}$$

The transverse aerodynamic load at the i^{th} element surface can be calculated by [19]:

$$F_{ai} = \frac{1}{2}\rho U^2 S_i c_{pi} \tag{19}$$

where ρ is the density of air, and S_i is the area of element surface i. The transverse load vector for all element surfaces is obtained by:

$$\mathbf{F_a} = \frac{1}{2}\rho U^2 \mathbf{S}\mathbf{c_p} \tag{20}$$

The main diagonal of the matrix **S** consists of elements areas. Substituting Eq. (18) into Eq. (20) gives:

$$\mathbf{F_a} = \frac{1}{2}\rho U^2 \mathbf{A}\mathbf{r}\mathbf{q_3} \tag{21}$$

where **Ar** is defined as:

$$\mathbf{Ar} = \mathbf{S}\mathbf{D}^{-1}\mathbf{v_{IT}} \tag{22}$$

Due to the symmetry of the wing, only the transverse aerodynamic loads on the half wing are calculated. Using the energy method, the concentrated transverse aerodynamic load vector at the doublet point of element surface i is obtained as follows [25, 26]:

$$\{\mathbf{F_{z0}}\}_i = F_{ai}\{\mathbf{a_3}(\xi_i, \eta_i)\}^T \tag{23}$$

For all elements of the half wing, Eq. (23) can be changed into as:

$$\mathbf{F_{z0}} = \sum_{i=1}^{N_e/2}\{\mathbf{F_{z0}}\}_i = \mathbf{a_3}\mathbf{F_a} \tag{24}$$

where $\mathbf{a_3}$ is a matrix whose columns are column vectors of Ritz trial functions at coordinates of the doublet points. The parameter N_e is the total number of element surfaces.
Substituting Eq. (21) into Eq. (24) yields:

$$\mathbf{F_{z0}} = \frac{1}{2}\rho U^2 \mathbf{a_3}\mathbf{A}\mathbf{r}\mathbf{q_3} \tag{25}$$

Finally, the equation of motion of the wing is obtained as:

$$M_w\,\ddot{\mathbf{q}}_{\mathbf{3}} + K_w\,q_3 = \frac{\mathbf{1}}{\mathbf{2}}\rho U^2\, a_3\, Ar\, q_3 \tag{26}$$

where $\mathbf{K_w}$ and $\mathbf{M_w}$ are sub-matrices of the stiffness and mass matrices of the wing corresponding to the transverse deflection [19, 25].

4 Flutter Analysis

wing motion is assumed harmonic, so $\mathbf{q_3}$ can be written as follows:

$$\mathbf{q_3} = \bar{\mathbf{q}}_3 e^{i\omega t} \tag{27}$$

where $\bar{\mathbf{q}}_3$ is the amplitude of the Ritz coefficients vector, and ω is the oscillation frequency of the wing. The reduced frequency k is defined as follows [29]:

$$k = \frac{b\omega}{U} \tag{28}$$

where b is semi-chord. By substituting Eq. (27) and Eq. (28) into Eq. (26) yields:

$$\mathbf{K_w}\bar{\mathbf{q}}_3 - \omega^2(\mathbf{M_w} + \bar{\mathbf{A}})\bar{\mathbf{q}}_3 = 0 \tag{29}$$

where $\bar{\mathbf{A}}$ is the aerodynamic matrix:

$$\bar{\mathbf{A}} = \rho\frac{b^2}{2k^2}\mathbf{a_3}\mathbf{A}\mathbf{r} \tag{30}$$

The U-g method is utilized to perform flutter analysis [29]. In this method, artificial structural damping g is added to the equation of motion, and flutter occurs when g=0 [11]. From Eq. (29) the eigenvalue problem can be written as:

$$\left[(1+ig)\mathbf{K_w} - \omega^2(\mathbf{M_w} + \bar{\mathbf{A}})\right]\bar{\mathbf{q}}_3 = 0 \tag{31a}$$

$$(Z\mathbf{K_w} - \bar{\mathbf{B}})\bar{\mathbf{q}}_3 = 0 \tag{31b}$$

Where

$$\bar{\mathbf{B}} = \mathbf{M_w} + \bar{\mathbf{A}} \tag{32}$$

And

$$Z = \frac{(1+ig)}{\omega^2} \tag{33}$$

The complex matrix $\bar{\mathbf{A}}$ is calculated for each value of reduced frequency k, and the complex eigenvalues Z is obtained from Eq. (31b). The ω, g, and U parameters are calculated as follows:

$$\omega = \sqrt{\frac{1}{Z(\mathrm{Re})}}, \mathrm{g} = \frac{Z(\mathrm{Im})}{Z(\mathrm{Re})}, U = \frac{\omega b}{k} \tag{34}$$

The value of the parameters ω and U at g=0 are the flutter frequency and flutter velocity, respectively [11].

5 Numerical Investigation and Discussion

The written MATLAB codes for vibration, aerodynamic, and aeroelastic analyses are validated, and used in a parametric study. The chordwise pressure coefficient distribution on a rectangular wing in unsteady flow is calculated, and then the vibration and flutter analyses of low aspect ratio composite wings are performed. The effects of wing sweep angle, aspect ratio, composite filament angle, and orthotropic modulus ratio on the flutter behavior of low aspect ratio composite wings in subsonic flow are investigated. The obtained results are verified with the results available in the literature.

A. Validation of the Written Aerodynamic Code

To validate the written aerodynamic code, a rectangular wing 2 meters by 4 meters oscillating in pitching motion around its mid-chord is studied. Real and Imaginary parts of the chordwise pressure coefficient distribution ($C_{P\alpha R}$ and $C_{P\alpha I}$) at the root and tip of the rectangular wing are shown in Figures (3-4), respectively (M=0, k=1, AR=2, N_x =5, N_y =10).

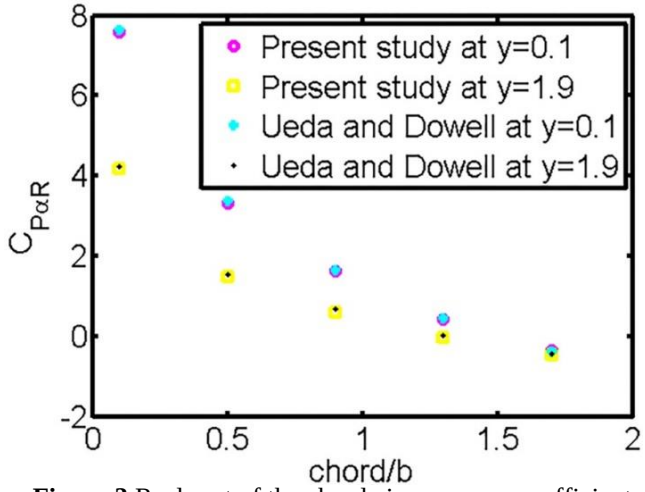

Figure 3 Real part of the chordwise pressure coefficient distribution at the root and tip of the rectangular wing

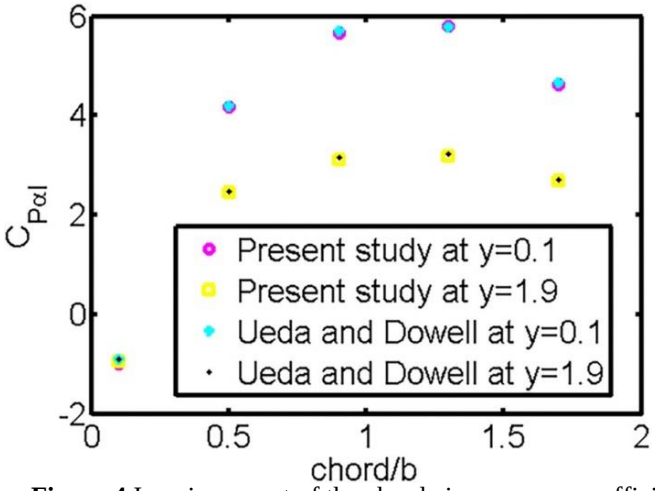

Figure 4 Imaginary part of the chordwise pressure coefficient distribution at the root and tip of the rectangular wing

Where N_x and N_y are the chordwise number of elements and one-half of the spanwise number of elements, respectively. The parameters M, AR, and α are Mach number of the uniform flow, aspect ratio of the wing, and angle of attack, respectively. The parameters $C_{P\alpha R}$, and $C_{P\alpha I}$ are real and imaginary parts of the chordwise pressure coefficient distribution, respectively. The presented results are similar to the results given by [10].

B. Free Vibration Analysis of a Semi-monocoque Main Wing with Low Aspect Ratio

The material and geometric parameters for the half-span representation of the isotropic wing shown in Figures (5-6) are as follows:
span = 4.88 m, tip width = 0.914 m, root width = 1.83 m, thickness = 0.0457 m, leading-edge sweep angle Λ=30 deg, mass density ρ = 2700 kg/m^3, Poisson's ratio v =0.3, and Young's modulus E =70.7 GPa. This wing is clamped at the root.
This wing has ten ribs and four spars distributed uniformly. Other particulars of the wing are presented in Table (1) as follows:

Table 1 Component properties of the Semi-monocoque wing

Structure	Properties, mm
rib/spar web	Thickness: 1.47
rib/spar cap	Width: 9.47 Height: 5
skin	Thickness: 3

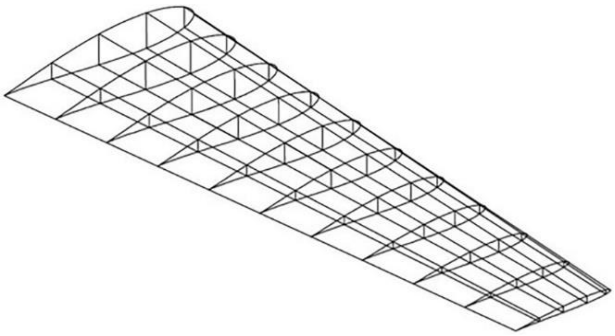

Figure 5 The semimonocoque wing

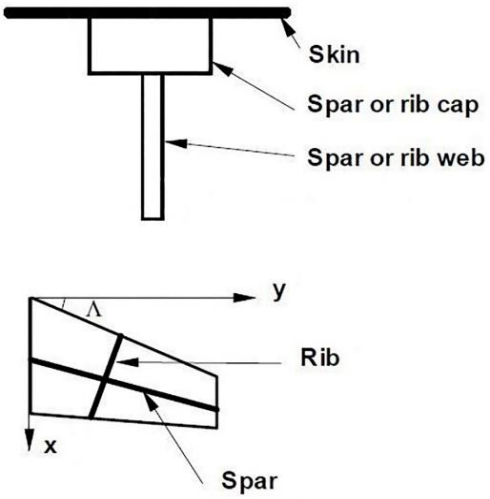

Figure 6 Wing spar or rib

Table 2 Natural frequencies of the semi-monocoque wing with NACA0021 airfoil, Hz

Mode Number	Present study	Equivalent plate method [30]	Error %	Nastran [30]	Error %
1	13.5 Bending	13.1 Bending	-3.1	12.9 Bending	-4.7
2	46.2 Inplane	-	-	47.7 Inplane	3.1
3	62.6 Bending	60.8 Bending	-3	56.6 Bending	-10.6
4	107.8 TLo*	-	-	68.1 TLo*	-58.3

*TLo: T – Torsion; Lo – Local

Natural frequencies of this semi-monocoque wing with NACA0021 aerofoil have been written in Table (2).

Mode shapes of the semi-monocoque wing with NACA0021 airfoil have been shown in Figure 7. The in-plane mode, which is mode number 2, has not been plotted in Figure (7).

The total freedom of this equivalent plate model is 320, and it requires only a few input data in comparison to a corresponding finite element model. The number of elements of the finite element model made by [30] in MSC/NASTRAN is 3784. Degrees of freedom of the equivalent plate model is 2% of degrees of freedom of the finite element model. Therefore, the calculation cost of the equivalent plate model is lower, and its preparation time is shorter than the finite element model.

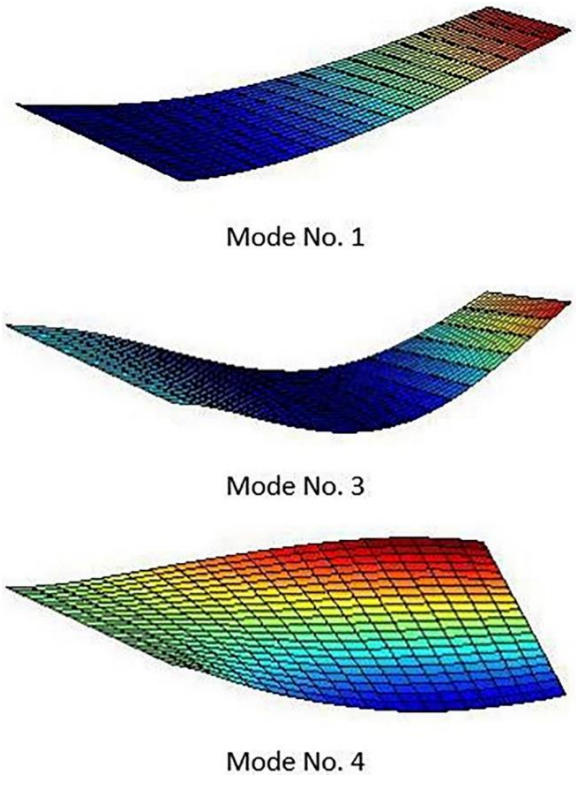

Figure 7 Mode shapes of the semi-monocoque wing with NACA0021 airfoil

C. Free Vibration Analysis of a Composite Wing with Low Aspect Ratio

Frequency parameters of a trapezoidal, symmetrically laminated $[-15/15/0]_s$ wing, $\Omega = (\omega a^2/h)\sqrt{\rho/E_2}$, with taper ratio = 0.25, quarter chord sweep angle γ = -45 deg, q =1, a/h = 10, are displayed in Table (3). The wing is made of a composite material with the following properties:
E_1/E_2 = 40, $G_{12}/E_2 = G_{13}/E_2$ = 0.6, G_{23}/E_2 = 0.5 and ν_{12} = 0.25.
where ν_{12} is the longitudinal Poisson's ratio and E_1, E_2, and G_{12} the longitudinal and transverse Young's moduli and the longitudinal shear modulus of unidirectional composites, respectively. The presented results in Table (3) are similar to those given by [25]. Mode shapes of the low aspect ratio composite wing have been shown in Figure (8). The in-plane mode, which is mode number (3), has not been plotted in Figure (8).

D. Flutter Performance of Low Aspect Ratio Composite Wings

The structural and air properties taken for this examination of a unidirectional low aspect ratio composite wing fluttering in air are listed below:
$E_2 = 4 \times 10^9$ N/m^2, ν_{12} =0.25, $G_{12} = 0.4\ E_2$, $\beta = E_1/E_2$
ρ_s = 1500 kg/m^3, t_s =0.016 m, ρ_a = 0.45908 kg/m^3, Sound speed = 303.2 m/s
The parameter β is defined as the orthotropic modulus ratio. ρ_s and t_s are the density and thickness of the wing, and ρ_a is the air density.

Table 3 Frequency parameter, $\Omega = (\omega a^2/h)\sqrt{\rho/E_2}$, for the first four frequencies of the above-mentioned low aspect ratio composite wing

Mode Number	Equivalent plate method **[25]**	Present study
1	7.5518	7.5518
2	15.948	15.948
3	24.892 In-plane mode	24.869 In-plane mode
4	27.817	27.817

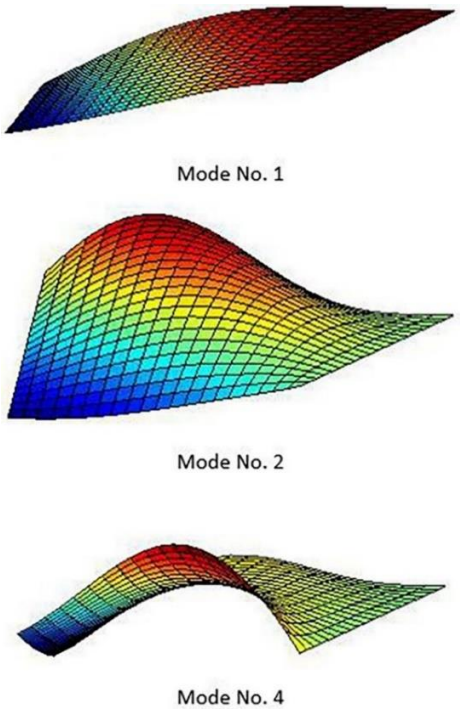

Figure 8 Mode shapes of the low aspect ratio composite wing

1. Effect of Composite Filament Angle

A flutter analysis is performed for several composite filament angles in the range of θ = 0-180 deg. Normalized flutter speeds are plotted in Figure (9). The results have good agreement with the results presented by [12].
Where V_F is the flutter speed, and V_R is the divergence speed at θ = 0 deg. As shown in Figure (9), it can be seen that by varying the composite filament angle θ, the dominant instability phenomenon exhibits an alternative flutter pattern. It is observed that high flutter speed generally occurs for θ <90 deg. This observation confirms the previous finding that the wing sweep angle has an opposite trend compared to the effect of the composite filament angle. It is concluded that the flutter characteristics of low aspect ratio composite wings are complicated; therefore, a parametric study is essential to determine that varying the directional stiffness is either beneficial or detrimental.

2. Effect of Orthotropic Modulus Ratio

Figure (10) shows the effect of orthotropic modulus ratio β on the flutter speeds of a wing with *AR*=1.5. The flutter speeds are normalized by the flutter speed of the isotropic case. An increasing β leads to increasing the flutter speed and vice versa. The presented results in Figure (10) have good agreement with the results given by [12].

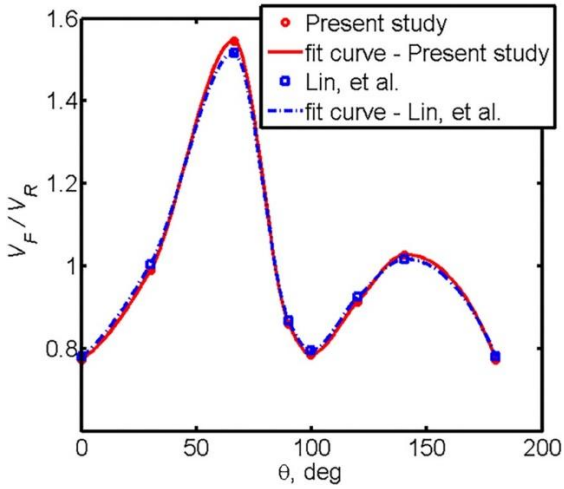

Figure 9 Normalized flutter speeds V_F/ V_R vs. composite filament angle θ for AR = 1.5 and β = 4 (V_R= 138.47 m/s = divergence speed at θ = 0 deg)

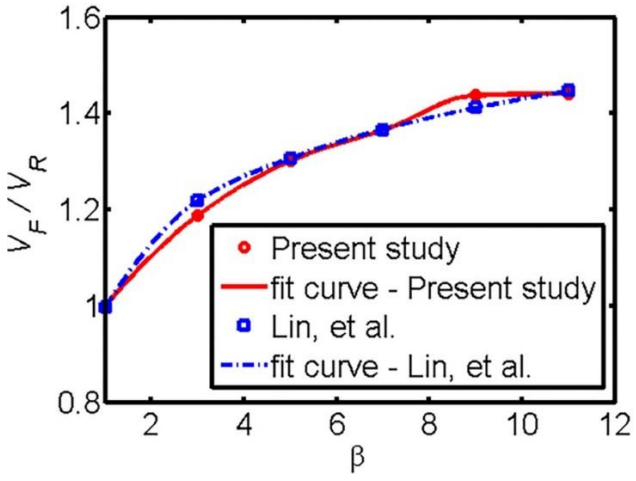

Figure 10 Normalized flutter speeds V_F/ V_R vs. orthotropic modulus ratio β for AR = 1.5 and θ=30º (V_R = 108.7 m/s)

3. *Effect of Sweep Angle*

The sweep angle effect for a low-aspect-ratio wing, AR = 1.5, is shown in Figure (11). The leading-edge sweep angle Λ is changed by rotating the wing, whereas keeping the wing area invariant. For swept-back wings, the flutter boundaries become lower. The presented results in Figure (11) have good agreement with the results given by [12].

4. *Effect of Aspect Ratio*

In Figures (12-13), the effects of aspect ratio AR on the flutter speeds are shown. Figure (12) shows the normalized speeds of the composite wing in different values of aspect ratio. It can be seen that the flutter speeds increase as AR decreases. In Figure (13), the percentage increments of flutter speeds of composite wings over the isotropic wing are illustrated (θ = 40º, β=8, and V_{F_i}= flutter speeds of the isotropic wing studied by[12].
From Figure (13), it is concluded that the considerable improvement upon flutter speeds is achieved by using composite materials, and the improvement upon flutter speeds is less sensitive to the AR value. The presented results in Figures (12-13) have good agreement with the results given by [12].

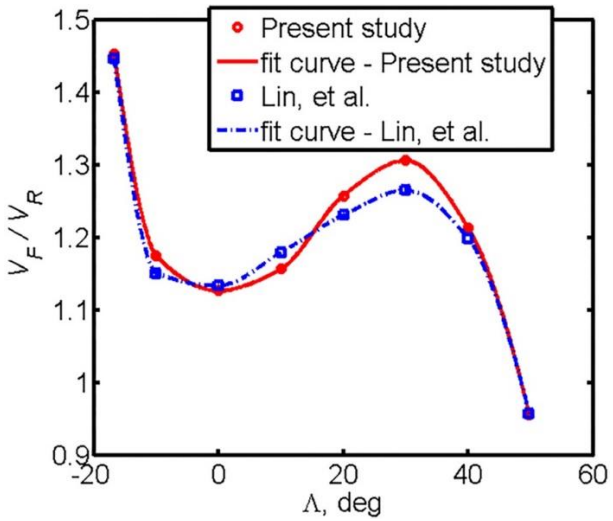

Figure 11 Normalized flutter speeds V_F/ V_R vs. sweep angle for the composite wing (θ = 40º, β=4 and V_R = 138.47 m/s = divergence speed at θ = 0 deg)

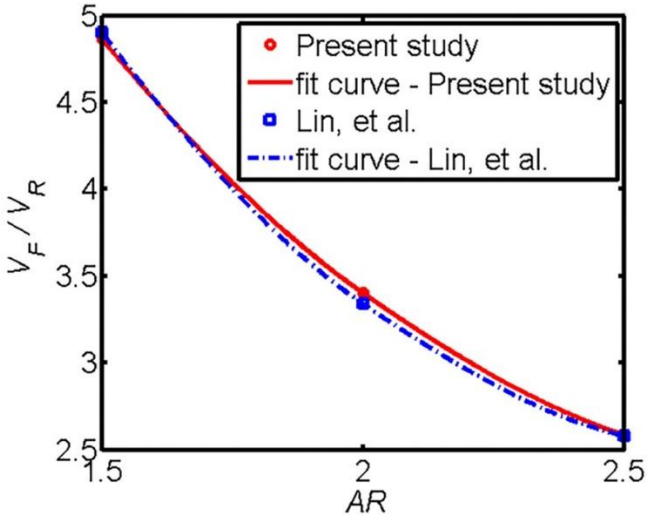

Figure 12 Normalized flutter speeds V_F/V_R vs. aspect ratio AR for the composite wing (θ = 40º, β=8 and V_R = 38.02 m/s = divergence speed at AR=4)

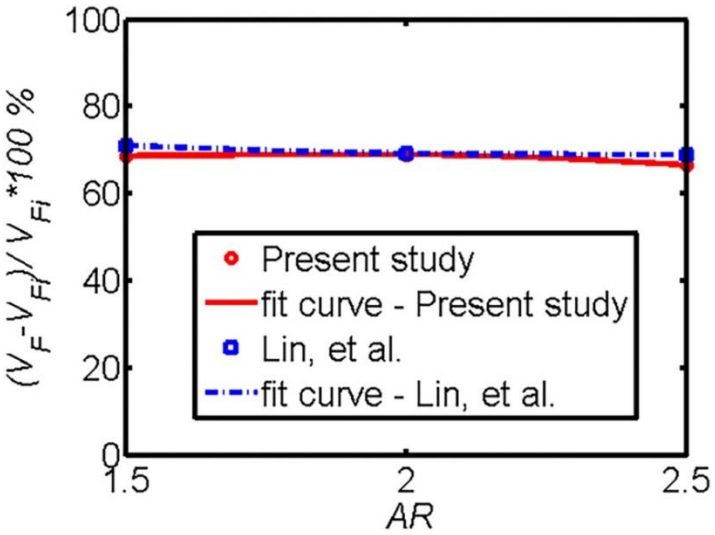

Figure 13 Percentage increment in flutter speeds of the composite wing vs. *AR* (θ = 40º, β=8).

6 Conclusion

An analytical investigation is proposed to study the flutter behavior of low aspect ratio composite wings in subsonic flow. The doublet point method is utilized to calculate unsteady aerodynamic load over the wing. An equivalent plate method is used for structural modeling of isotropic and composite low aspect ratio wings. Chebyshev polynomials are applied in the Rayleigh-Ritz method as trial functions, and the first-order shear deformation theory is utilized to formulate the structural deformation. Boundary conditions are enforced by applying proper artificial springs. Flutter analysis is performed using the U-g method.

Achieving both effective analysis and fast modeling in free vibration and flutter analysis of low aspect ratio composite wings in the preliminary design stage instead of using the computationally expensive FEM are purposes of the present approach. This approach requires only a few numbers of the input data and has a short runtime relative to a finite element model. The effects of sweep angle, aspect ratio, composite filament angle, and orthotropic modulus ratio on the flutter behavior of composite wings in subsonic flow are investigated. The flutter speeds show a wavelike trend as the composite filament angle changes, almost with the 90 deg of phase shift. An increasing the orthotropic modulus ratio leads to increasing the flutter speed while aspect ratio has an opposite effect. The structural tailoring can make a harmonious balance to the sweep angle effect upon the flutter behavior of a composite wing. By properly tailoring the wing structure, it is possible to achieve considerable improvement upon flutter performance. The obtained results are verified with the results available in the literature.

The presented approach will be developed for flutter analysis of a composite semi-monocoque wing with a control surface.

References

[1] Wright, J., and Cooper, J.J.A., "*Introduction to Aircraft Aeroelasticity and Loads*", 2nd Edition, Courier Dover Publications, New York, pp. 123-139, (2007).

[2] Krishnamurthy, T., and Mason, B., "Equivalent Plate Analysis of Aircraft Wing with Discrete Source Damage", 47th AIAA/ASME/ASCE/AHS/ASC Structures, Structural Dynamics, and Materials Conference,14th AIAA/ASME/AHS Adaptive Structures Conference 7th, May 1-4, Newport, Rhode Island, USA, pp. 2218, (2006).

[3] Fung, Y.C., "*An Introduction to the Theory of Aeroelasticity*", 3rd Edition, Courier Dover Publications, New York, pp. 186-187, (2008).

[4] Kussner, H., "General Airfoil Theory", Report 19930094437, NACA TM-979, (1941).

[5] Watkins, C.E., Woolston, D.S., and Cunningham, H.J., "A Systematic Kernel Function Procedure for Determining Aerodynamic Forces on Oscillating or Steady Finite Wings at Subsonic Speeds", Report 118098417, NASA TR-R-48, (1959).

[6] Redman, M., and Rowe, W., "Prediction of Unsteady Aerodynamic Loadings Caused by Leading Edge and Trailing Edge Control Surface Motions in Subsonic Compressible Flow", Report 107297721, NASA CR-2543, (1975).

[7] Albano, E., and Rodden, W.P., "A Doublet-lattice Method for Calculating Lift Distributions on Oscillating Surfaces in Subsonic Flows", AIAA Journal, Vol. 7, pp. 279-285, (1969).

[8] Blair, M., "A Compilation of the Mathematics Leading to the Doublet Lattice Method", Report 116860505, WL-TR-92-3028, (1992).

[9] Rodden, W.P., Taylor, P.F., and McIntosh Jr, S.C., "Further Refinement of the Subsonic Doublet-lattice Method", Journal of Aircraft, Vol. 35, pp. 720-727, (1998).

[10] Ueda, T., and Dowell, E., "A New Solution Method for Lifting Surfaces in Subsonic Flow", AIAA Journal, Vol. 20, pp. 348-355, (1982).

[11] Hollowell, S.J., and Dugundji, J., "Aeroelastic Flutter and Divergence of Stiffness Coupled, Graphite/Epoxy Cantilevered Plates", Journal of Aircraft, Vol. 21, pp. 69-76, (1984).

[12] Lin, K.-J., Lu, P.-J., and Tarn, J.-Q., "Flutter Analysis of Cantilever Composite Plates in Subsonic Flow", AIAA Journal, Vol. 27, pp. 1102-1109, (1989).

[13] Koo, K., and Lee, I., "Aeroelastic Behavior of a Composite Plate Wing with Structural Damping", Computers and Structures, Vol. 50, pp. 167-176, (1994).

[14] Abdelrahmen, W., "Static and Dynamic Behaviour of Composite Swept Wings", M.Sc. Thesis, Department of Aerospace Engineering, Cairo University, Cairo, (1995).

[15] Dunn, P., and Dugundji, J., "Nonlinear Stall Flutter and Divergence Analysis of Cantilevered Graphite/Epoxy Wings", AIAA Journal, Vol. 30, pp. 153-162, (1992).

[16] Livne, E., and Li, W.-L., "Aeroservoelastic Aspects of Wing/Control Surface Planform Shape Optimization", AIAA Journal, Vol. 33, pp. 302-311, (1995).

[17] Lu, P.-J., and Huang, L.-J., "Flutter Suppression of Thin Airfoils using Active Acoustic Ecitations", AIAA Journal, Vol. 30, pp. 2873-2881, (1992).

[18] Na, Y.-H., and Shin, S., "Equivalent-plate Analysis for a Composite Wing with a Control Surface", Journal of Aircraft, Vol. 50, pp. 853-862, (2013).

[19] Abbas, M.K., Negm, H.M., and Elshafei, M.A., "Flutter and Divergence Characteristics of Composite Plate Wing", International Conference on Aerospace Sciences and Aviation Technology, May 28-30, Cairo, Egypt, pp. 1-21, (2013).

[20] Jian, T., Changchuan, X., and Chao, Y., "Flutter Analysis of Aircraft Wing using Equivalent-plate Models with Orthogonal Polynomials", Transactions of Nanjing University of Aeronautics and Astronautics, Vol. 32, pp. 5, (2015).

[21] Saeed, S., and Salman, S., "Flutter Analysis of Hybrid Metal-composite Low Aspect Ratio Trapezoidal Wings in Supersonic Flow", Chinese Journal of Aeronautics, Vol. 30, pp. 196-203, (2017).

[22] Babin, T., and Sangeetha, N., "Flutter Analysis of Supersonic Low Aspect Ratio Composite Wings using FSI Methodology", Advances in Manufacturing Processes, September 11, Singapore, pp. 361-372, (2019).

[23] He, X., Song, Z., Wu, Z., and Liu, F., "Aeroelastic Testing for Freeplay Induced Limit Cycles of Flexible Wing-aileron System", AIAA Scitech 2020 Forum, January 6-10, Orlando, USA, pp. 21-31, (2020).

[24] Pohly, J.A., Zhang, M.R., and Zhang, S., "Wing Flutter Analysis using Computational Fluid-structure Interaction Dynamics", ASME 2021 Fluids Engineering Division Summer Meeting, August 10–12, Virtual, Online, pp. 1-8, (2021).

[25] Kapania, R.K., and Lovejoy, A.E., "Free Vibration of Thick Generally Laminated Cantilever Quadrilateral Plates", AIAA Journal, Vol. 34, pp. 1474-1486, (1996).

[26] Kapania, R.K., and Liu, Y., "Static and Vibration Analyses of General Wing Structures using Equivalent-plate Models", AIAA Journal, Vol. 38, pp. 1269-1277, (2000).

[27] Lovejoy, A.E., "Natural Frequencies and an Atlas of Mode Shapes for Generally-laminated, Thick, Skew, Trapezoidal Plates", M.Sc. Thesis, Department of Aerospace Engineering, University of Virginia, Virginia, (1994).

[28] Crawley, E.F., Curtiss, H.C., Peters, D.A., Scanlan, R. H., and Sisto, F., "*A Modern Course in Aeroelasticity*", 4th Edition, Springer, New York, pp. 246, (1995).

[29] Bisplinghoff, R.L., Ashley, H., and Halfman, R.L., "*Aeroelasticity*", 2nd Edition, Courier Corporation, New York, pp. 545-551, (2013).

[30] Na, Y.-H., Kim, J.-H., and Shin, S.-J., "Vibration Analyses of an Equivalent Plate Wing with an External Store", The Aeronautical Journal, Vol. 118, pp. 1090-1098, (2014).

Nomenclature

a_3 vector of the trial functions in Ritz method
AR aspect ratio of a wing
b semi-chord (m)
c_p vector of pressure coefficient
D matrix of aerodynamic influence coefficients
F_{z0} column vector of the aerodynamic load
g artificial structural damping
h thickness of the wing (m)
k reduced frequency
K stiffness matrix
K kernel function
M Mach number of a uniform flow

M mass matrix
N_e total number of element surfaces
N_x chordwise number of elements
N_y one-half of the spanwise number of elements
q time-dominant Rayleigh-Ritz coefficients vector
S region of the wing area
U uniform flow speed (m/s)
V_F flutter speed (m/s)
V_R divergence speed (m/s)
w_0 transverse deflection (m)
Z complex eigenvalues

Greek symbols

γ quarter chord sweep angle (deg)
Δ_i area of an element surface (m^2)
Δ_p nondimensional amplitude of pressure differential
θ composite fiber angle
Λ leading-edge sweep angle (deg)
ρ_∞ density of the uniform flow (kg/m^3)
σ_i one-half width of an element surface (m)
ω oscillation frequency (rad/s)

Subscripts

i i^{th} element surface
α angle of attack (deg)

Appendix

Flutter diagrams (damping coefficient vs. air flow speed and frequency vs. air flow speed) for a composite wing (θ = 40º, Λ = 30º, β=8) are plotted in Figure (I).

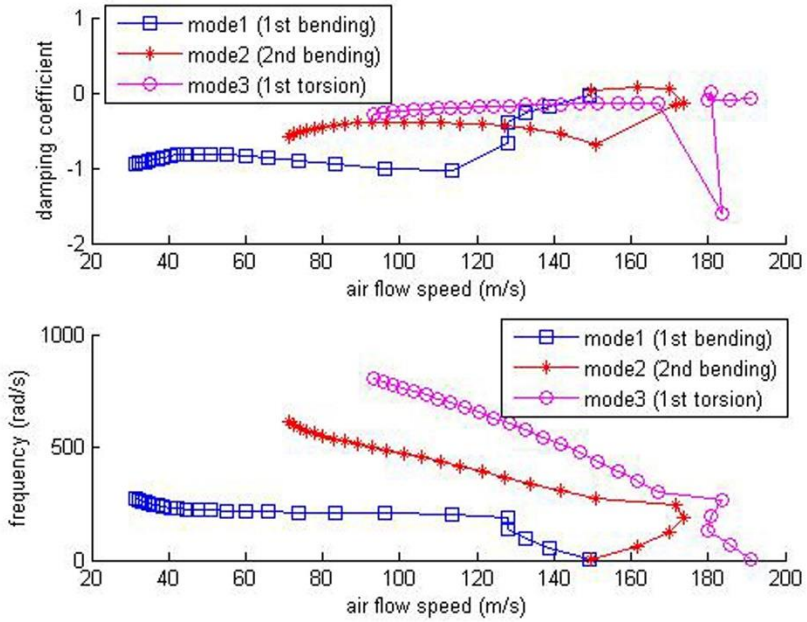

Figure I damping coefficient vs. air flow speed and frequency vs. air flow speed (θ = 40º, Λ = 30º, β=8)